Synthesis and Characterization of Polymethacrylamide–Clay Nanocomposites

R. Anbarasan, P. Arvind, V. Dhanalakshmi

Department of Polymer Technology, Kamaraj College of Engineering and Technology, Virudhunagar 626 001, Tamil Nadu, India

Received 16 June 2010; accepted 28 October 2010
DOI 10.1002/app.33622
Published online 22 February 2011 in Wiley Online Library (wileyonlinelibrary.com).

ABSTRACT: Polymethacrylamide intercalated hectorite clay nanocomposites were synthesized by the *in situ* free-radical polymerization method. The interlayer cation of hectorite clay was modified with cetyl pyridinium chloride and cetrimide, and their effects on the rate of polymerization of methacrylamide and the structure–property relationships of the resulting polymer nanocomposites were investigated. Fourier transform infrared spectroscopy showed a peak around 550 cm^{-1} that was due to the metal oxide stretching of hectorite clay in the polymer nanocomposites. High-resolution transmission electron microscopy determined the size of polymethacrylamide as 300 nm. X-ray diffraction was used for the determination of the intercalated products. © 2011 Wiley Periodicals, Inc. J Appl Polym Sci 121: 563–573, 2011

Key words: clay; FT-IR; glass transition; nanocomposites

INTRODUCTION

Nanoscience is an interdisciplinary field that seeks to bring about mature nanotechnology. Focusing on the nanoscale intersection of fields such as physics, biology, engineering, chemistry, and computer science, nanoscience is expanding rapidly. Nanotechnology centers are popping up around the world. The rapid progress is apparent by the increasing appearance of the prefix *nano* in scientific journals and news. Nanosized materials are very useful in various science and engineering fields, particularly in the polymer field, for increasing the thermal stability, mechanical properties, flame retardancy, electrical conductivity, and crystallinity too. In this investigation, nanosized materials were used to improve the thermal stability of a polymer through their surface catalytic effects. The synthesis and characterization of highly crosslinked polyacrylamides and polymethacrylamide (PMAm) were reported.[1] Misra and Dubey[2] studied the redox-initiated aqueous polymerization of methacrylamide (MAm). A report on the crystal structure effect in the radiation-induced solid-state polymerization of MAm is available in the literature.[3] Gupta and Behari[4] published the results on the peroxydisulfate/malonic acid redox-pair-initiated polymerization of MAm. PMAm and poly(itaconic acid) complexes were prepared and characterized by Fourier transform infrared (FTIR) spectroscopy, thermogravimetric analysis (TGA), and elemental analysis.[5] Gallardo and San Ronan[6] reported the results of the synthesis and characterization of a new PMAm bearing side groups for biomedical interests. Apart from PMAm, some of its derivatives have also been reported.[7–16] Ultrasound (US) is one of the nondestructive methods used for different purposes in chemistry,[17–24] particularly in the field of polymer chemistry.[22,24] US is useful to human beings in many ways. In this investigation, US was used to accelerate the modification process of hectorite clay (HC) with different surfactants. A PMAm/sodium montmorillonite nanocomposite was synthesized by the free-radical polymerization method.[25] In a thorough literature survey; we did not find any report with PMAm–HC nanocomposites. In this article, we report the modification of HC in the presence and absence of US. Typically, MAm was polymerized by an *in situ* method in the presence of modified clay. FTIR spectroscopy, TGA, differential scanning calorimetry (DSC), X-ray diffraction (XRD), and high-resolution transmission electron microscopy (HRTEM) techniques were used to characterize the resulting polymer nanocomposites.

EXPERIMENTAL

Materials

MAm (Ottokemi, Analar grade, India) was purchased and polymerized after a recrystallization process. Potassium persulfate (PDS; Ottokemi) was used

Correspondence to: R. Anbarasan (anbu_may3@yahoo.co.in).

as an initiator. Ascorbic acid (AA; Sisco, India) was used as a reducing agent. HC [$Na_{0.6}(Li_{0.6}Mg_{54})Si_8O_{28}Cl_4$] was collected from our institution's campus and was purified with acid and base washing. Cetyl pyridinium chloride (CPC; Sisco) and cetrimide (CET; Sisco) were purchased and were used as received without any further purification. A gun-type Branson 1020, USA model ultrasonicator with a frequency of 20,000 KHz was used.

Structural modification of HC

Purified clay (10 g) was placed with 1000 mL of double-distilled (DD) water into a beaker. CPC or CET (10 g) was added with vigorous stirring at 75°C for 12 h under a nitrogen atmosphere. During the ion-exchange reaction, the Li^+ ion present in the interlayer space of HC underwent an ion-exchange reaction with CPC or CET. The thus-obtained structurally modified clay was filtered and washed with DD water three times and was dried at 110°C for 12 h. The resulting substance was washed with DD water until the filtrate showed a pH of 7.0. The dried mass was weighed and stored in a zipper bag. The same procedure was adopted for the structural modification of clay in the presence of US.

Synthesis of PMAm

PMAm was synthesized by a solution polymerization method. A 1*M* solution of MAm (20 mL) was pipetted into a 250-mL, round-bottom flask along with freshly prepared solutions of 0.05*M* PDS (20 mL) and 0.05*M* AA (20 mL). DD water (40 mL) was added to the solution. This mixture was subjected to vigorous stirring under a nitrogen atmosphere at 75°C for 6 h. After the polymerization reaction, the contents were poured into 100 mL of methanol. The thus-formed PMAm was precipitated, filtered, and dried at 60°C for 24 h *in vacuo.* This polymer sample was taken as a control. The same procedure was adopted for the synthesis of the PMAm nanocomposites in the presence of modified or unmodified clay.

The rate of polymerization (R_p) was calculated as follows:

$$R_p = \frac{W_p}{VtM} \times 1000 \quad (1)$$

where W_p is the weight of the obtained polymer, V is the total reaction volume, t is the reaction time (s), and M is the molecular weight of MAm.

Characterization

FTIR characterization was done with a Shimadzu FTIR 8400 S, Japan model instrument by the KBr pelletization method from 400 to 4000 cm^{-1}. TGA and DSC were carried out with an STA 409 simultaneous TGA and DSC, (TA instruments) analysis system at a heating rate of 10°C/min under nitrogen and air atmospheres for DSC and TGA, respectively. XRD was carried out with an advanced instrument (Bruker XS08 model instrument) by scanning from the 2θ value of 2 to 60° at a scanning rate of 2°/min. HRTEM was recorded with a JEOL TEM 3010, USA instrument.

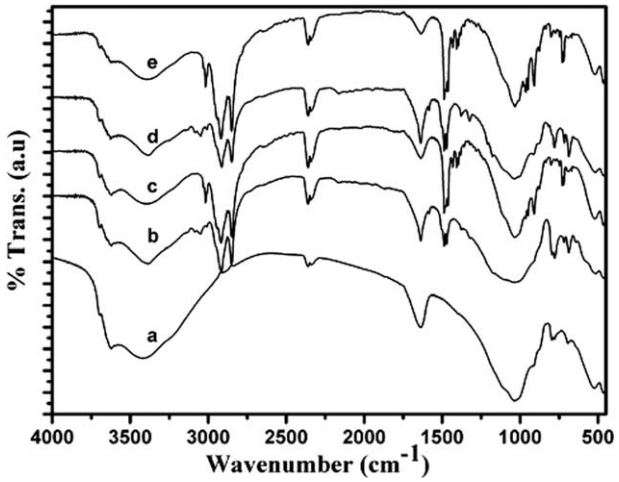

Figure 1 FTIR spectra of (a) clay, (b) clay–CET, (c) clay–CET–US, (d) clay–CPC, and (e) clay–CPC–US systems.

RESULTS AND DISCUSSION

Our aim was to study the effect of modified or unmodified clay on R_p of MAm and the thermal stability of the resulting polymer nanocomposites. For the preparation of the polymer nanocomposites, the clay was used as a nanomaterial (unmodified and modified forms). For that purpose, we used two different structural modifiers in the presence and absence of US. By analyzing their properties, we concluded that the hybrids prepared in the presence of US showed better efficiency, and hence, we used the same hybrid for the preparation of the polymer nanocomposites. Hence, this investigation was subdivided into two parts, namely, (1) the synthesis and characterization of the hybrids and (2) the synthesis and characterization of the polymer nanocomposites.

Characterization of the hybrids

FTIR spectroscopy

The FTIR spectrum of pristine clay is shown in Figure 1(a). The metal oxide stretching was observed at 550 cm^{-1}. The peak at 1631 cm^{-1} was due to the bending vibration of water molecules associated with clay. The broad peak around 3400 cm^{-1} was

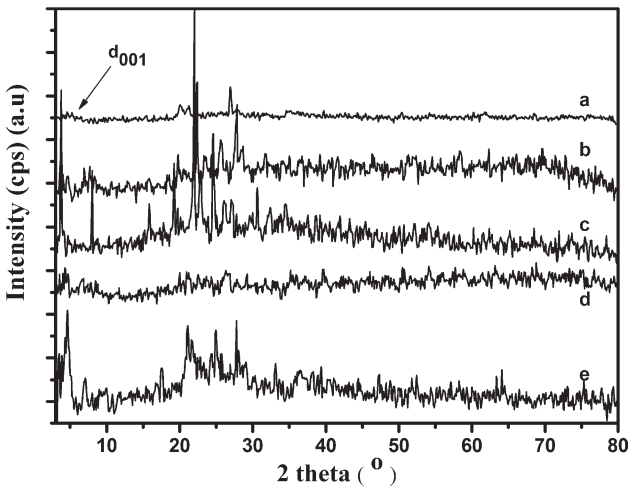

Figure 2 XRD for (a) clay, (b) clay–CET, (c) clay–CET–US, (d) clay–CPC, and (e) clay–CPC–US.

due to the OH stretching. Intermolecular hydrogen bonding was observed at 3630 cm^{-1}. The FTIR spectrum of CET-modified clay is shown in Figure 1(b). Here, one can also see the aforementioned peaks with some additional new peaks. The peaks at 1639 and 1484 cm^{-1} explained the carbonyl stretching, and that at 1380 cm^{-1} was ascribed to the C—N stretching of CET. A twin peak that appeared at 2838 and 2912 cm^{-1} corresponded to the C—H symmetric and antisymmetric stretching vibrations, respectively. Figure 1(c) shows the FTIR spectrum of the clay–CET–US system. This spectrum was similar to that of the clay–CET system. Figure 1(d,e) shows the FTIR spectra of the clay–CPC and clay–CPC–US hybrid systems, respectively. Here also, the previously mentioned peaks appeared. Hence, the structural modification of the clay through the intercalation reaction of CET or CPC in the presence and absence of US was confirmed.

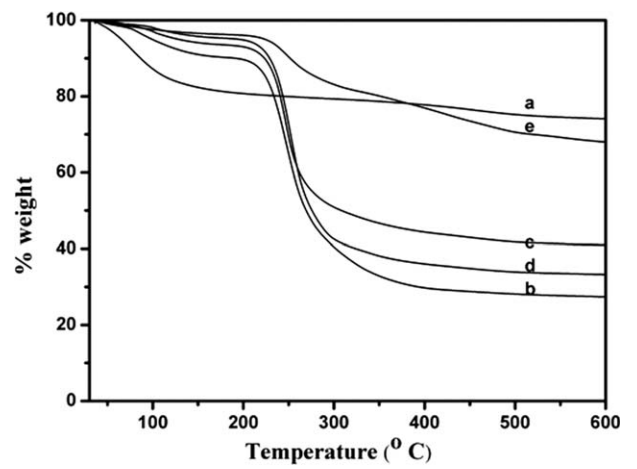

Figure 3 TGA for (a) clay, (b) clay–CET, (c) clay–CET–US, (d) clay–CPC, and (e) clay–CPC–US.

TABLE I
TGA Results for the Clay Hybrid Systems

System	wt %			
	100°C	300°C	500°C	>550°C
Clay	87.47	79.30	75.39	73.83
Clay–CET	94.68	40.97	28.17	27.27
Clay–CET–US	96.96	50.82	41.39	41.09
Clay–CPC	98.16	42.65	34.10	33.10
Clay–CPC–US	97.62	82.96	70.58	68.01

XRD profile

Figure 2 shows the XRD results of HC before and after the modification process. The raw HC was modified with CET (1 : 1 ratio) or CPC (1 : 1 ratio). HC showed [Fig. 2(a)] a d_{001} plane peak at 4.96°, which was responsible for the increase in the basal spacing of HC. The other crystal plane peaks were available at very low intensities. When the clay was modified with CET, XRD showed some new peaks in the lower 2θ ranges. The appearance of a peak at 3.56° [Fig. 2(b)] confirmed the intercalation of CET into the basal spacing of HC. The other crystal planes showed the improved crystallinity of clay–CET. The same intercalation reaction was carried out in the presence of CET with US assistance. In Figure 2(c), we observed a sharp peak at 3.56° with an increase in intensity. This confirmed that US accelerated the modification process through its cavitations mechanism.[22] Recently, Anbarasan et al.[26] modified the structure of LDH with different functionalities in the presence of US. XRD of the final hybrid showed an improved crystalline peak. The structure of HC was modified with CPC, both in the absence [Fig. 2(d)] and in the presence [Fig. 2(e)] of US. This system also explained the role of US during the structural modification of clay. In the overall comparison, the structural modification of clay in the presence of US showed higher crystalline peaks than in its absence. Moreover, the increase in basal spacing was very low because of the parallel alignment of CET or CPC inside the basal spacing of the clay.

TGA history

TGA informed us about the thermal stability of the clay. Figure 3(a) shows the TGA results for the pristine clay. Pristine clay showed a single-step degradation process because of the removal of moisture and physisorbed water molecules.[27] Table I presents the residues (weight percentages) at different temperatures. Above 550°C, 73.8 wt % residue remained. When the clay was modified with CET (in the absence of US), the thermogram showed a two-step degradation process [Fig. 3(b)]. The first minor weight loss step up to 200°C was due to the

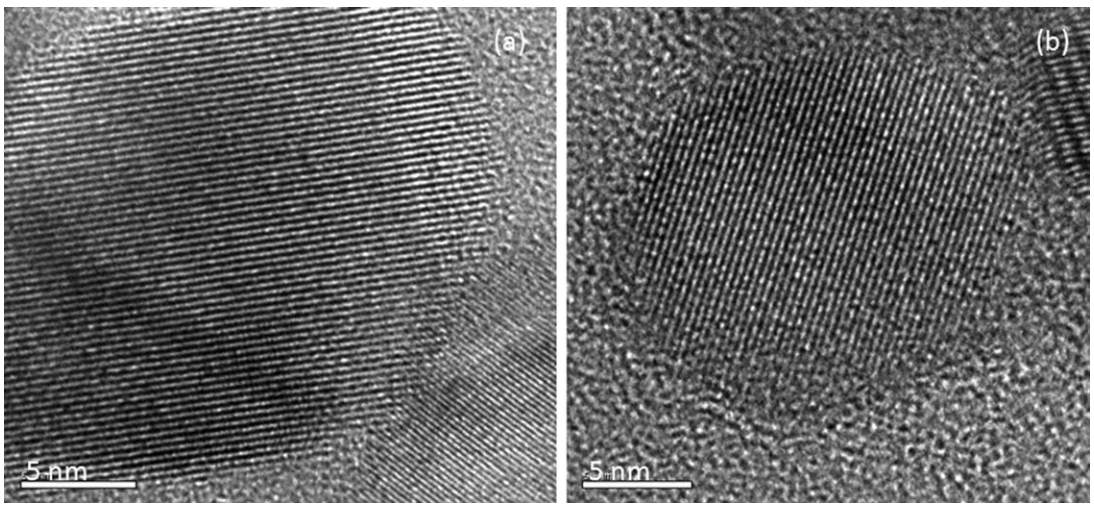

Figure 4 HRTEM images of the raw clay.

removal of both physisorbed and chemisorbed water molecules. The second major weight loss step up to 300°C was associated with the breaking of the hybrid structure, and it retained a weight of 27.27% at 550°C (Table I). Clay was modified with CET in the presence of US [Fig. 3(c)]. This system showed a two-step degradation process, as mentioned previously. However, the weight percentage of residue above 550°C was increased to 41.09 wt %. The increase in the thermal stability was explained on the basis of the increase in the stereoregular arrangement of intercalant in the basal spacing of clay with the assistance of US. Figure 3(d) indicates the TGA results for the CPC-modified clay system (in the absence of US). The thermogram showed a two-step degradation process. The weight percentage of residue remaining above 550°C was 33.1% (Table I). The TGA results for the US-assisted modification of clay with CPC are shown in Figure 3(e), and the data for the weight percentage of residue above 550°C as 68.01% are shown in Table I. The US-assisted process increased the thermal stability of the clay–CPC hybrid system through the stereoregular arrangement of the intercalant in the basal spacing of clay. In comparison, the CPC–clay system exhibited a higher thermal stability than the clay–CET system; particularly, the CPC–clay–US system showed a higher thermal stability.

HRTEM study

Figure 4 shows the HRTEM images of the pristine clay. Figure 4(a,b) shows a nanorod-like morphology with a length of about 15 nm and a breadth of 0.3 nm. These nanorods were nothing but the various crystal planes of HC. Various crystal planes were arranged in a perfect manner without any distortion. Figure 5 indicates the HRTEM images of US-assisted, CET-modified clay. The hybrid had porous structure 3–5 nm wide [Fig. 5(a,c)]. Figure 5(b) indicates the agglomerated portion, too. The layered structure of silicates was disturbed by the intercalant [Fig. 5(d)], CET, and the topography showed a wormlike morphology. Figure 6 shows the HRTEM images of US-assisted, CPC--modified clay with an exfoliated morphology. The layer structure of clay was broken into platelets with lengths of 5–10 nm [Fig. 6(a)]. The exfoliated clay platelets had a length of 3 nm [Fig. 6(b)]. Because of exfoliation, some spherical morphologies [Fig. 6(c)] with a porous structure about 10 nm wide [Fig. 6(d)] was observed. The US-assisted, CPC--modified clay exhibited a spherelike morphology.

Characterization of the polymer–clay nanocomposites

Effects of [MAm], the weight percentage of clay, the weight percentage of clay–CET, the weight percentage of clay–CET–US, the weight percentage of clay–CPC, and the weight percentage of clay–CPC–US on R_p

We polymerized MAm at different concentrations under a nitrogen atmosphere at 75°C for 6 h by keeping the other experimental conditions constant. When the MAm concentration was increased, the R_p values increased. To determine the order of the polymerization reaction, plots between log [MAm] and log R_p [Fig. 7(a)] were made, and the slope values were determined as 0.81. The slope value confirmed a first-order polymerization reaction with respect to [MAm]. This led to the unimolecular termination reaction.[17,22]

The effects of modified and unmodified clay on R_p of MAm were tested with different weight percentage loadings. When the loading of pristine clay was increased from 1 to 5 wt %, the R_p value increased

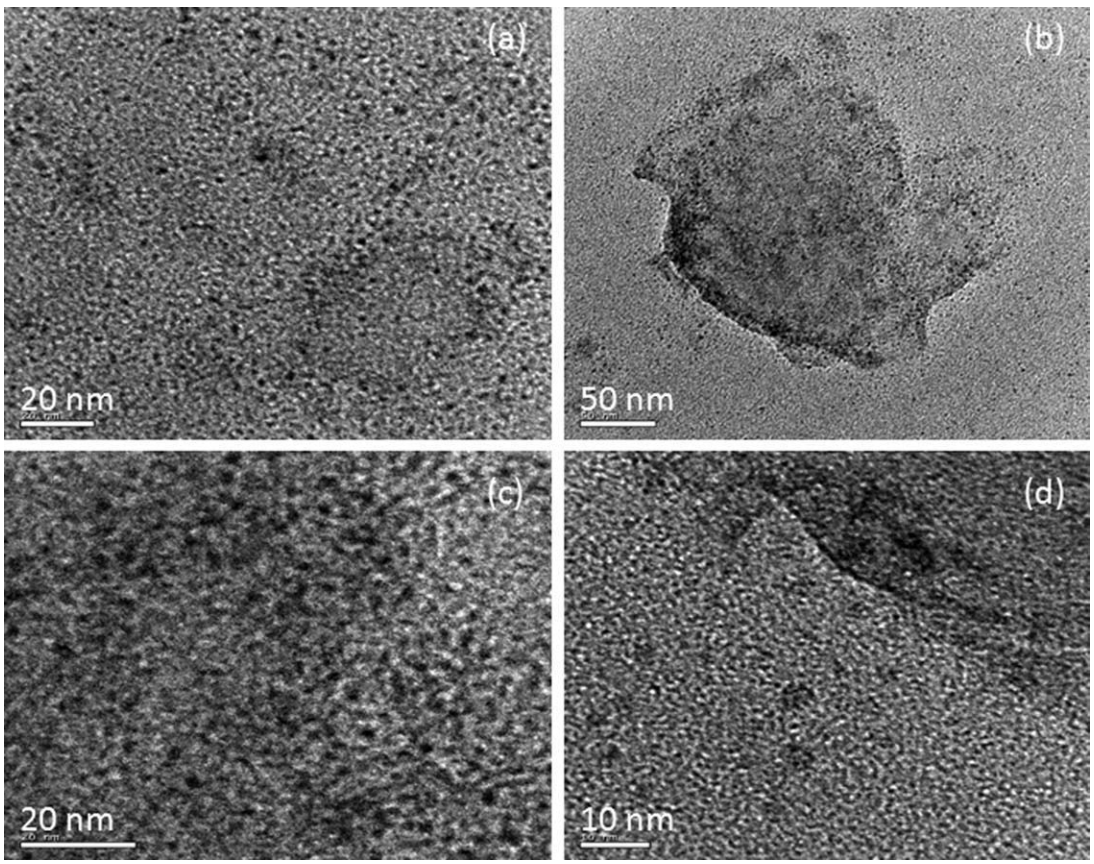

Figure 5 HRTEM images of clay–CET–US.

slowly at first. Above a 3 wt % loading of clay, there was a rapid increase in R_p. This was due to the following reasons: (1) the surface catalytic activity of the clay, (2) hydrophilicity with a greater water-retention capacity, and (3) uniform interaction between the clay and monomer. To determine the order of the polymerization reaction, a log–log plot was made, that is, a plot of the logarithm of the weight percentage of clay versus log R_p [Fig. 7(b)]. The plot showed two regions, and the slope value was determined in region II as 0.50. This indicated that the nanosized clay catalyzed the polymerization of MAm and followed the 0.50 order of reaction with respect to the weight percentage of clay. It indicated that 0.50 mol of clay was required to initiate 1 mol of MAm monomer in the presence of the PDS–AA redox system. This confirmed the catalytic activity of the nanosized clay. Similar plots were made for CET- and CPC-modified-clay-catalyzed polymerizations of MAm in both the presence and absence of US [Fig. 7(c–f)]. The slope values were determined as 0.31 (clay–CET), 0.25 (clay–CET–US), 0.48 (clay–CPC), and 0.33 (clay–CPC–US) for this investigation. This implied that the clay–CET–US system catalyzed the polymerization of MAm and obeyed the 0.25 order of reaction with respect to the weight percentage of clay–CET–US. Similarly, the clay–CPC–US system exhibited a 0.50 order of reaction with respect to the weight percentage of clay–CPC–US. The pristine clay and clay–CPC–US systems effectively catalyzed the polymerization of MAm because of their hydrophilic nature in contrast to the clay–CET–US system. The decrease in the order of reaction for the clay–CET–US system was due to the existence of the more hydrophilic nature of the hybrid, which interacted more with the monomeric units. In comparison, in the presence of US, both of the surfactants showed a lower order of reaction because of the exfoliation or intercalation effect. Moreover, in the presence of US, a lesser quantity of modified clay was required to initiate 1 mol of monomer. In the absence of clay, 1 mol of initiator was required to initiate 1 mol of monomer unit, but in the presence of the clay (either in the modified or unmodified form), a lesser quantity of initiator (PDS) was required for initiation purposes because of the cocatalyzing nature of the clay (because of its surface catalytic effect). The effect of HC on the chemical polymerization of aniline was examined by our research team, and we demonstrated the catalytic effect of HC.[28] Recently, our research team proved that the HC could catalyze the

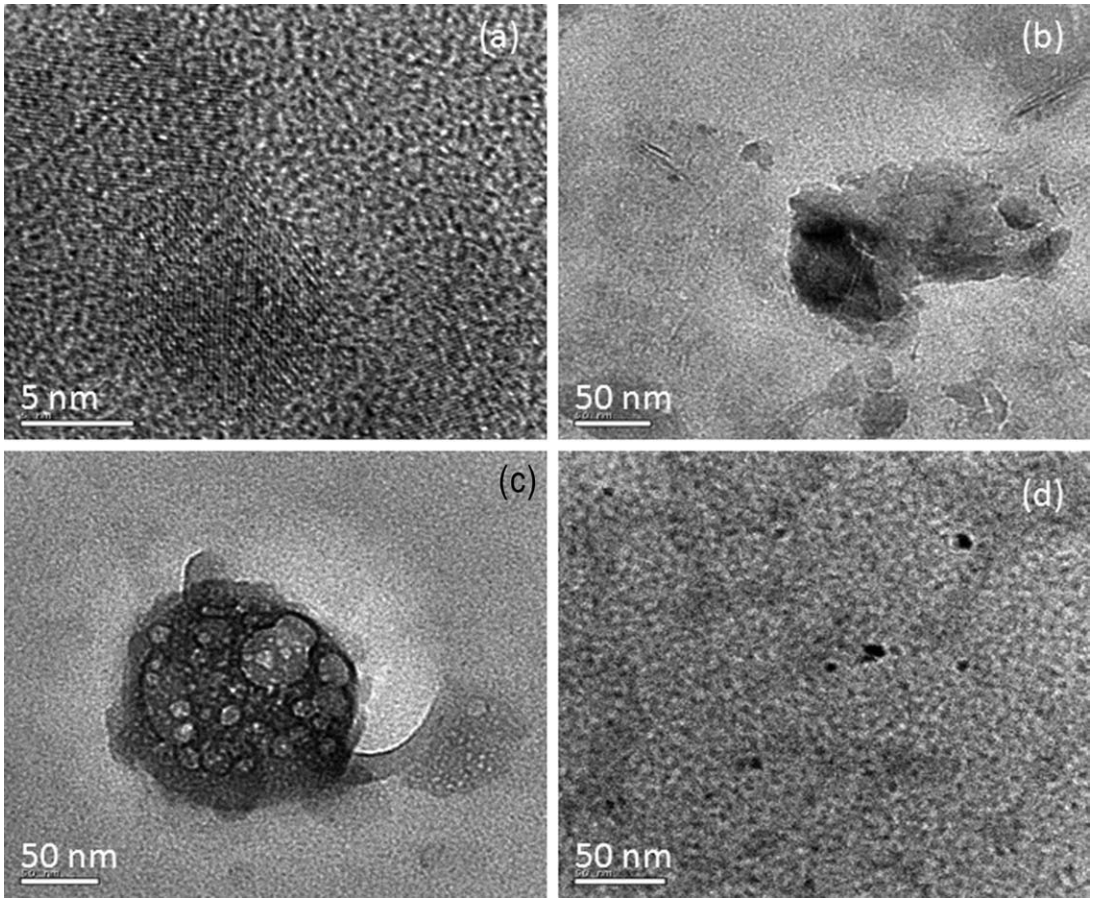

Figure 6 HRTEM images of clay–CPC–US.

condensation polymerization of glycolic acid.[29] The effects of unmodified and modified clays on the molecular weight of PMAm through GPC are under investigation in our research laboratory. By a trial-and-error method, we fixed the weight percentage loading of clay in the modified and unmodified forms during the *in situ* polymerization of MAm at 5%. At a higher weight percentage loading of the clay (particularly, >5 wt % loading), agglomeration was observed, with a reduction in the polymer yield. Our ultimate aim was to increase the thermal properties of PMAm with an increase in the percentage yield by the surface catalytic effect of the nanosized clay. Hence, we optimized the weight percentage clay loading at 5 wt % only. Our earlier communication also reflected the same factor.[28]

FTIR spectroscopy of the polymer nanocomposites

The FTIR spectrum of pristine PMAm is shown in Figure 8(a). The N—H stretching vibrations were observed at 3412 cm^{-1}. OH stretching was observed around 3207 cm^{-1} because of the presence of water molecules intermolecularly associated with PMAm. The C—H symmetric and antisymmetric stretching vibrations were observed at 2944 and 2986 cm^{-1}, respectively. The carbonyl stretching and bending vibrations of water molecules were observed at 1665 and 1598 cm^{-1}, respectively. The C—H out-of-plane bending vibrations appeared at 1199 cm^{-1}. The PMAm nanocomposites also exhibited the same

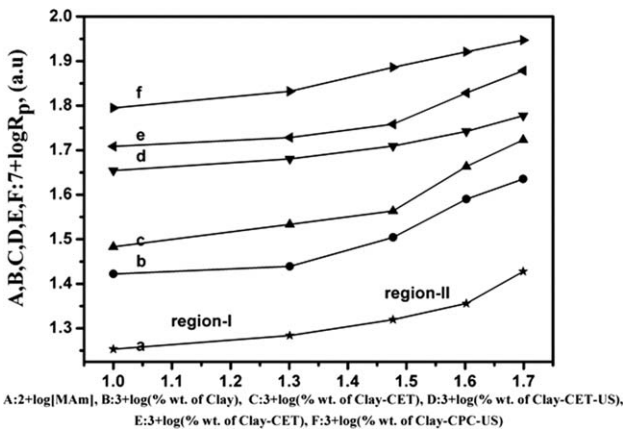

Figure 7 Effects of (a) the MAm concentration, (b) the weight percentage of clay, (c) the weight percentage of clay–CET, (d) the weight percentage of clay–CET–US, (e) the weight percentage of clay–CPC, and (f) the weight percentage of clay–CPC–US on R_p (time = 6 h, temperature = 75°C, [PDS] = 0.05*M*, [AA] = 0.05*M*).

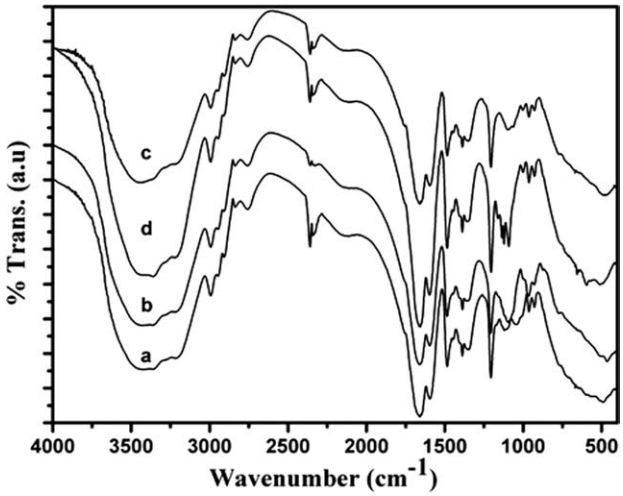

Figure 8 FTIR spectra of (a) PMAm, (b) PMAm–clay, (c) PMAm–clay–CET–US, and (d) PMAm–clay–CET–US.

peaks [Fig. 8(b–d)]. A new peak around 550 cm^{-1} explained the M—O stretching vibrations. This confirmed the presence of metal oxide stretching in the PMAm–clay nanocomposite system.

DSC and TGA results for PMAm

Figure 9(a) shows the DSC thermogram of PMAm. The thermogram indicated an endothermic peak at 66.7°C and implied the removal of physically adsorbed water molecules from the PMAm surface. The presence of water molecules on the PMAm surface was confirmed earlier by FTIR spectroscopy. Figure 9(b) shows the TGA results for pristine PMAm. It showed a three-step degradation process. The first minor weight loss step up to 110°C was associated with the removal of moisture and water molecules from PMAm. This supported the FTIR spectroscopy and DSC reports for the presence of water molecules on the PMAm surface. The second minor weight loss

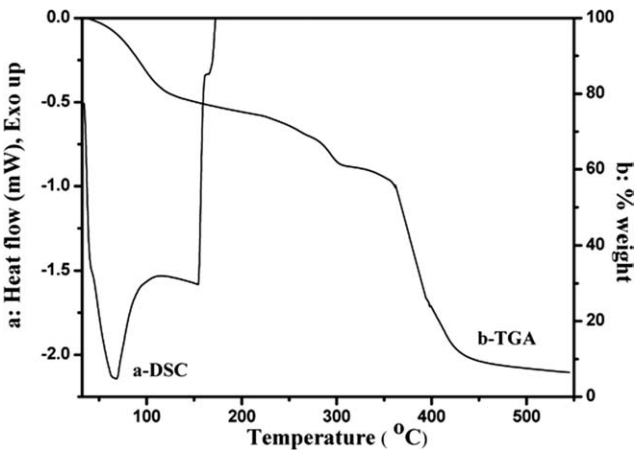

Figure 9 (a) DSC and (b) TGA for PMAm.

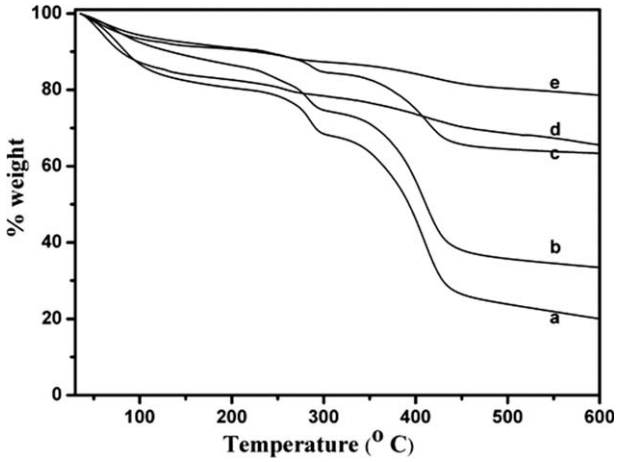

Figure 10 TGA for PMAm loaded with clay: (a) 1, (b) 2, (c) 3, (d) 4, and (e) 5 wt %.

step up to 315°C was attributed to the breaking of intermolecular and intramolecular hydrogen bonding and to the slight degradation of the amide linkage in PMAm. The third major weight loss around 385°C was due to the degradation of the PMAm backbone. Above 550°C, 5 wt % remained; this showed the slight char-forming behavior of PMAm. This was in accordance with Onal and Celik's[27] report.

TGA for the PMAm–clay nanocomposites

The TGA results for PMAm with different weight percentage loadings of clay are shown in Figure 10. The thermogram showed a three-step degradation process, similar to pristine PMAm. It was noted that when the weight percentage of clay increased, the weight percentage remaining above 550°C increased. PMAm with 5 wt % clay showed the highest thermal stability; that is, PMA loaded with 5 wt % clay exhibited 79 wt % residue remaining above 550°C. This was due to the intercalation of PMAm chains into the basal spacing of the clay. Moreover, at a higher weight percentage loading of clay, the intermolecular hydrogen bonding and PMAm chain degradation were stabilized because of the crosslinking nature of the PMAm gel.[1] This showed that the PMAm–clay nanocomposite system was a thermally stable material. The data are mentioned in Table II.

TABLE II
TGA Results for the PMAm–Clay Nanocomposites

System	wt %			
	100°C	300°C	500°C	>550°C
PMAm–clay (1 wt %)	99.76	68.11	46.07	21.44
PMAm–clay (2 wt %)	92.33	74.85	56.40	34.11
PMAm–clay (3 wt %)	94.14	84.84	74.91	63.42
PMAm–clay (4 wt %)	87.30	78.53	73.54	67.39
PMAm–clay (5 wt %)	93.73	87.40	84.15	79.97

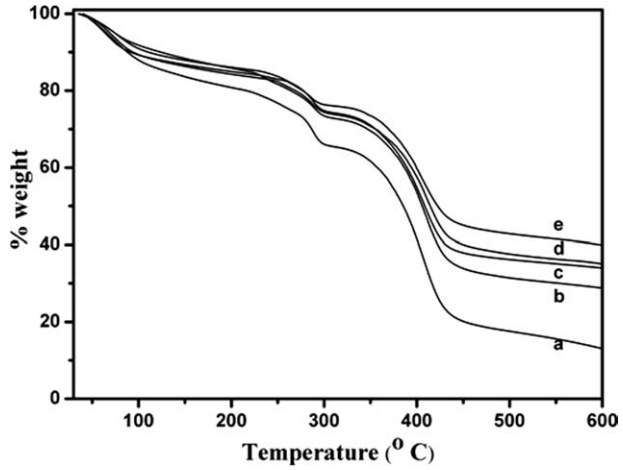

Figure 11 TGA for PMAm loaded with clay–CET–US: (a) 1, (b) 2, (c) 3, (d) 4, and (e) 5 wt %.

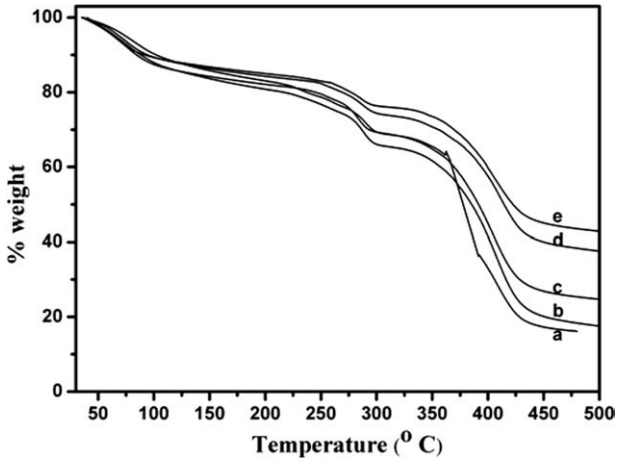

Figure 12 TGA for PMAm loaded with clay–CPC–US: (a) 1, (b) 2, (c) 3, (d) 4, and (e) 5 wt %.

In 2007, Kvien et al.[30] reported the thermal and mechanical properties of starch/HC nanocomposite systems. They implied that the added HC increased the thermal and mechanical properties of starch because of the intercalation process. Our results coincided with those of their systems. The thermal stability of the CET–US-modified clay system loaded at different weight percentages during the *in situ* polymerization of MAm is shown in Figure 11. Again, the polymer nanocomposite showed a three-step degradation process, as mentioned earlier. The important point here is that when the weight percentage of clay–CET–US was increased, the weight percentage residue remaining above 550°C increased (Table III). This explained the char-forming capability of the polymer nanocomposite systems.

Figure 12 indicates the TGA results for the PMAm–clay–CPC–US system. When the weight percentage loading of clay–CPC–US increased, the weight percentage residue remaining above 450°C also increased (Table IV). The maximum char-forming stability was obtained at a 5 wt % loading of the clay–CPC–US system with 44.16 wt % residue. In comparison, the PMAm–clay system showed the highest thermal stability of the systems. The order was as follows on the basis of the char-forming activity: PMAm–clay > PMAm–clay–CPC–US > PMAm–clay–CET–US > PMAm.

HRTEM for the PMAm–clay nanocomposites

Figure 13 shows the topography of the PMAm nanocomposite system loaded with 5 wt % raw clay. Figure 13(a) shows the PMAm intercalated layered structure of the clay after the *in situ* polymerization reaction; this can be seen in the shaded area. Figure 13(b) indicates the exfoliated clay platelets. A distorted spherical morphology of the clay about 50 nm in length [Fig. 13(c)] was observed. Moreover, the polymer chain size was about 250–300 nm [Fig. 13(d)]. As a result of nanocomposite formation, the size of the PMAm was reduced from the micrometer to the nanometer scale; that is, during the *in situ* polymerization of MAm in the presence of clay, the size of the macropolymer itself was reduced. This was due to the influence of the nanosized clay, which acted as a host matrix for PMAm. The surface catalytic effect of clay also played a vital role here.

Figure 14 shows the HRTEM images of the US assisted, CET-modified clay in a PMAm matrix. One can see the exfoliated layered structure of clay after the *in situ* polymerization reaction [Fig. 14(a)]. Figure 14(b) indicates the topography of PMAm with a length of about 200 nm. During the structural modification of the clay, both US and the reaction temperature acted as driving forces for the

TABLE III
TGA Results for the PMAm–Clay–CET–US Systems

System	wt %			
	100°C	300°C	500°C	>550°C
PMAm–clay–CET–US (1 wt %)	87.93	65.86	41.57	13.76
PMAm–clay–CET–US (2 wt %)	92.30	73.41	53.90	29.40
PMAm–clay–CET–US (3 wt %)	90.76	74.85	54.53	34.30
PMAm–clay–CET–US (4 wt %)	89.77	75.35	58.27	35.52
PMAm–clay–CET–US (5 wt %)	87.93	76.10	58.71	40.42

TABLE IV
TGA Results for the PMAm–Clay–CPC–US Systems

System	wt %			
	100°C	300°C	500°C	>550°C
PMAm–clay–CPC–US (1 wt %)	90.30	69.45	33.11	16.23
PMAm–clay–CPC–US (2 wt %)	87.52	65.95	41.07	17.76
PMAm–clay–CPC–US (3 wt %)	87.43	69.14	44.69	25.12
PMAm–clay–CPC–US (4 wt %)	89.64	74.44	58.18	37.98
PMAm–clay–CPC–US (5 wt %)	89.14	76.60	60.11	42.88

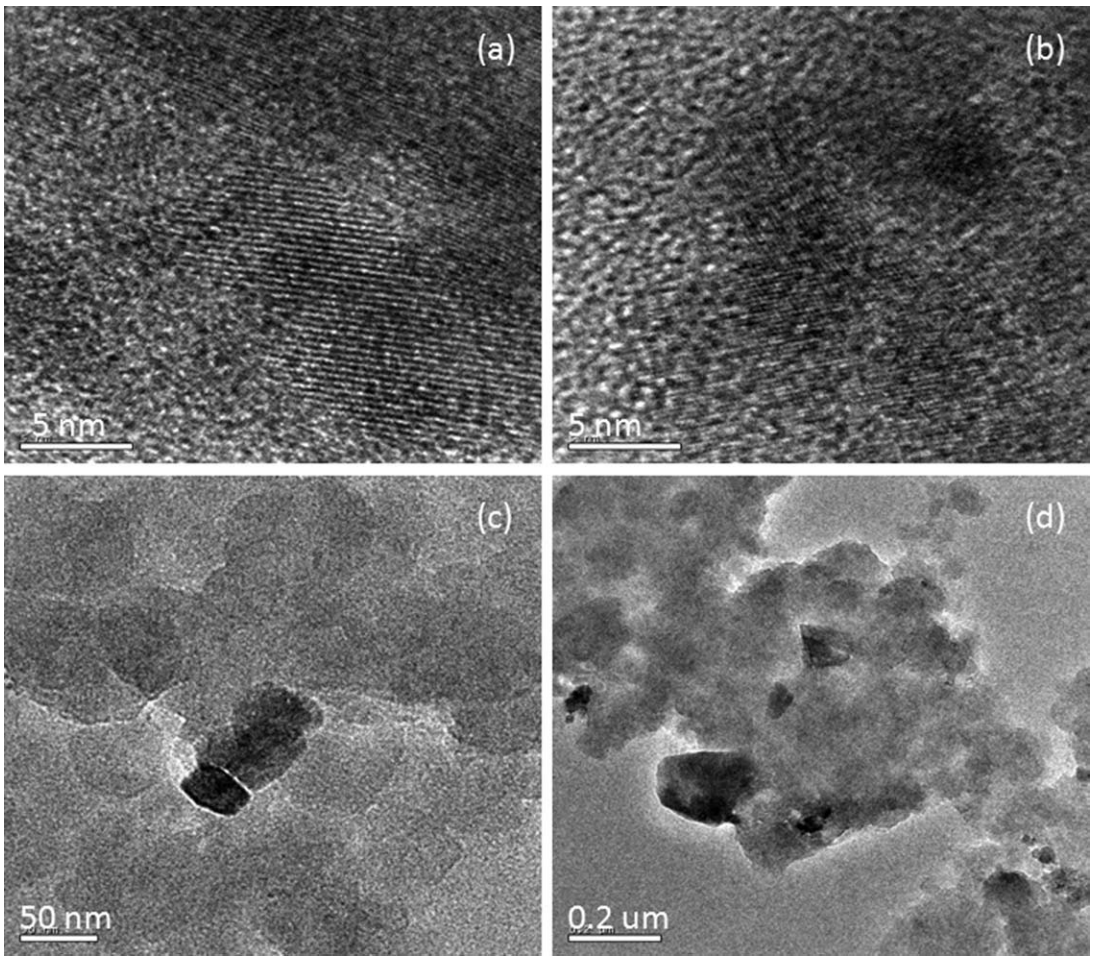

Figure 13 HRTEM images of the PMAm–clay (5 wt %) system.

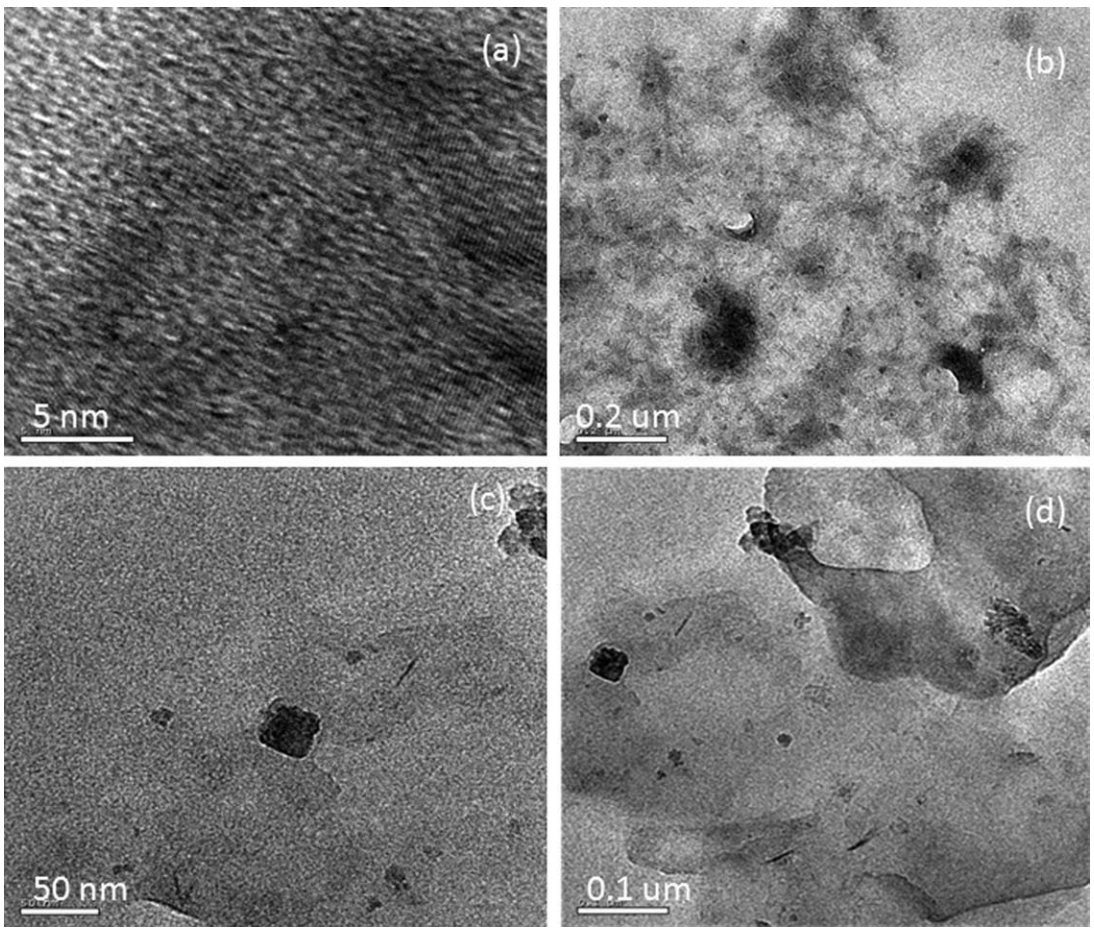

Figure 14 HRTEM images of the PMAm–clay–CET–US (5 wt %) system.

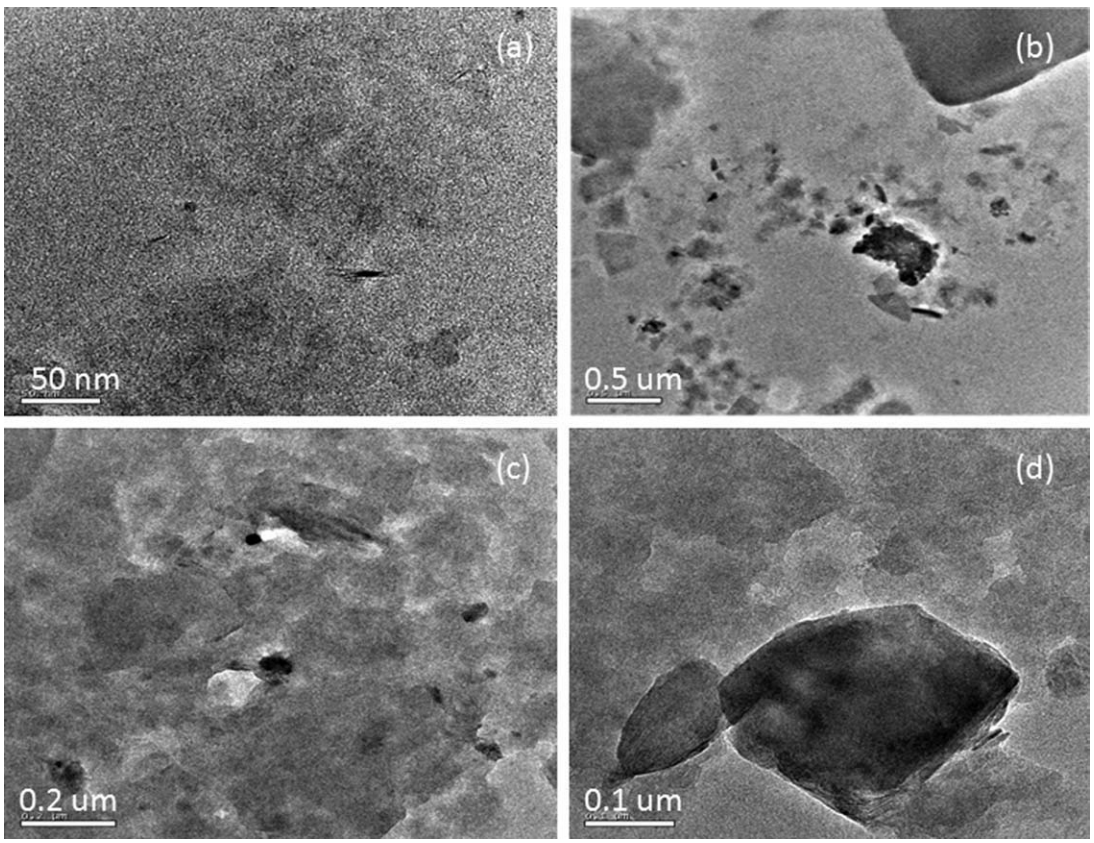

Figure 15 HRTEM images of the PMAm–clay–CPC–US (5 wt %) system.

intercalation of the surfactant into the interlayer space of the clay. Furthermore, during the *in situ* polymerization reaction, the intercalated polymer chains exfoliated the clay platelets. Figure 14(c) shows the agglomerated platelets with a length of 25 nm and a breadth of 25 nm. The distribution of the exfoliated clay platelets in the PMAm matrix is shown in Figure 14(d).

Figure 15 shows the HRTEM images of the PMAm–clay–CPC–US (5 wt % loaded) system. The clay platelets were broken and dispersed here and there in the PMAm matrix [Fig. 15(a)]. Again, both US and the reaction temperature acted as driving forces for the penetration of the surfactant into the basal spacing of the clay. During the *in situ* polymerization reaction, the polymer chains grew between the layers of the clay, and this resulted in a nanosized polymer with a length of about 300 nm [Fig. 15(b)]. Again, the PMAm size was suppressed to 300 nm in the presence of the CPC-modified clay; this decreased the size of the polymer. This confirmed that the modified clay controlled the size and growth of PMAm and that the clay platelets acted as nucleating agents. Figure 15(c) shows the dispersion of the clay platelets on the nanosized PMAm matrix. The agglomerated PMAm, with a length of about 300 nm and a breadth of 250 nm, is shown in Figure 15(d).

CONCLUSIONS

From this study, we summarize the following important points here as conclusions:

1. US-assisted structural modification of clay showed an improved crystallinity and higher thermal stability; these were evidenced from XRD and TGA, respectively.
2. HRTEM confirmed the size of clay as 15 nm.
3. The polymerization of MAm followed a first-order reaction, whereas the polymerization in the presence of the US–clay–CPC hybrid exhibited a 0.50 order of reaction with respect to the weight percentage loading of clay.
4. When the weight percentage loading of the pristine clay was increased, the thermal stability increased and reached a maximum at 5 wt % loading.
5. DSC confirmed the dewatering temperature of PMAm as 66.7°C.
6. HRTEM confirmed the exfoliated morphology of the clay and showed that it was dispersed on the PMAm matrix uniformly.
7. Among the clays used for the preparation of the polymer nanocomposites, the pristine clay exhibited the highest thermal stability because of the existence of strong interactions between the polymer and the clay.

8. During the *in situ* polymerization reaction, the size of PMAm was suppressed to about 300 nm. This suggested that during the nanocomposite preparation, a nanosized polymer was also produced with excellent thermal stability.

References

1. Shea, K. J.; Stoddard, G. J.; Choate, R. M. Macromolecules 1990, 23, 4497.
2. Misra, G. S.; Dubey, S. C. Colloid Polym Sci 1979, 257, 156.
3. Usamanz, A.; Kafadar, A. B. J Macromol Sci Pure Appl Chem 2004, 41, 387.
4. Gupta, K. C.; Behari, K. Polym Bull 1986, 16, 109.
5. Krusic, M. K.; Whuzovi, E. D.; Filipovi, J. Eur Polym J 2004, 40, 793.
6. Gallardo, A.; San Ronan, J. Polymer 1993, 34, 394.
7. Hazot, P.; Chapel, J. P.; Delair, J. J Polym Sci Part A: Polym Chem 2002, 40, 1808.
8. Fakhrul, A. K. M.; Kamigairo, M.; Okamoto, Y. Polym J 2006, 38, 1035.
9. Kobayashi, M.; Kirata, M.; Takeshi, M. Polym J 2004, 36, 238.
10. Liang, J. L.; Bell, J. P.; Scola, D. A. J Appl Polym Sci 1993, 48, 477.
11. Chen, R.; Benicewicz, B. C. Macromolecules 2003, 36, 6333.
12. Ulbrich, K. J Bioact Compos Polym 2000, 15, 4.
13. Celik, M. A. J Polym Res 2006, 13, 427.
14. Kahira, T. N.; Fann, L.; Boon, C. T.; Yoshikumi, M. Polym J 1998, 30, 910.
15. Kumar, S. K.; Hong, J. D.; Lim, C. K. Macromolecules 2006, 39, 3217.
16. Saimon, E.; Shaari, A. H.; Rahman, A.; Susilavati, A. Am J Appl Sci 2005, 2, 1248.
17. Vivekanandam, T. S.; Gopalan, A.; Umapathy, S. J Appl Polym Sci 2000, 76, 524.
18. Challis, R. E. Annu Rev Mater Sci 1999, 29, 295.
19. Richards, W. T.; Loomis, A. C. J Am Chem Soc 1927, 49, 3086.
20. Porter, C. V.; Young, L. J Am Chem Soc 1938, 60, 1497.
21. Algera, T. J.; Kleverlaan, C. J.; Feilze, A. J. Eur J Orthod 2005, 27, 472.
22. Anbarasan, R.; Jeyaseharan, J.; Gopalan, A. J Appl Polym Sci 2003, 89, 3685.
23. Anbarasan, R.; Lee, W. D.; Im, S. S. Bull Mater Sci 2005, 28, 145.
24. Constable, G. S.; Bryan, C. J Polym Sci Part B: Polym Phys 2003, 41, 1323.
25. Liu, L. S.; Kost, J.; Langer, R. Macromolecules 1992, 25, 123.
26. Anbarasan, R.; Lee, W. D.; Im, S. S. J Serb Chem Soc 2008, 73, 321.
27. Onal, M.; Celik, M. Mater Lett 2006, 60, 48.
28. Anbarasan, R.; Gopiganesh, C. Int J Polym Mater 2006, 55, 803.
29. Durai Murugan, K.; Baskaran, I.; Anbarasan, R. Chin J Polym Sci 2008, 26, 393.
30. Kvien, I.; Sugiyama, J.; Votrubec, M.; Oksman, K. J Mater Sci 2007, 42, 8163.